Geophysical Research Letters®

Key Points:

- The extratropical response to the Madden-Julian Oscillation has changed on decadal time scales
- This decadal variability coincides with changes in low-frequency oceanic modes in both the Pacific and Atlantic basins
- Changes on decadal time scales are different to those modulated by the El Niño-Southern Oscillation on interannual scales

Supporting Information:

Supporting Information may be found in the online version of this article.

Correspondence to:

D. T. Skinner,
D.Skinner@uea.ac.uk

Decadal Variability of the Extratropical Response to the Madden–Julian Oscillation

Daniel T. Skinner[1] [ID]**, Adrian J. Matthews[1,2]** [ID]**, and David P. Stevens[1]** [ID]

[1]Centre for Ocean and Atmospheric Sciences, School of Mathematics, University of East Anglia, Norwich, UK, [2]Centre for Ocean and Atmospheric Sciences, School of Environmental Sciences, University of East Anglia, Norwich, UK

Abstract The Madden–Julian Oscillation (MJO) is the leading mode of sub-seasonal variability in the tropical atmosphere and is a source of predictability for extratropical weather through its teleconnections. MJO teleconnection patterns can be modulated by the El Niño–Southern Oscillation (ENSO) on seasonal to interannual time scales. However, changes over decadal time scales are less well understood. ERA5 reanalysis data are used to show that the boreal winter MJO teleconnection pattern in the Northern Hemisphere has changed in recent decades in line with changes in the Pacific Decadal Oscillation and Atlantic Multidecadal Variability. Changes are seen in the circulation, temperature and precipitation responses. In particular, from 1997, intraseasonal cold anomalies appear over Europe and the eastern United States due to MJO convection over the western Pacific; these were not present 20 years previously. The decadal variability observed is not the product of aliasing of ENSO modulation of the teleconnection.

Plain Language Summary Weather in different regions of the globe can be linked by planetary-scale atmospheric waves, and these links can help forecasters to predict the weather. One such link, or teleconnection pattern, connects changes in rainfall over Indonesia and the tropical Pacific (from a weather system called the Madden–Julian Oscillation or MJO) to changes in the weather in North America and Europe. This study assesses this teleconnection pattern in two separate time periods (roughly the mid-1970s to mid-1990s and mid-1990s to late 2010s) to analyze if and how it has changed. We find that the pattern has changed, and that this is due to large-scale changes in the background state of the atmosphere. These changes in the link between the tropics and extratropics will have implications for weather forecasts on weekly to monthly time scales.

1. Introduction

As the leading mode of sub-seasonal variability in the tropical atmosphere, the Madden–Julian Oscillation (MJO; Madden & Julian, 1971; Madden & Julian, 1972) can influence weather around the globe (Jiang et al., 2020; Lin, 2022; Matthews et al., 2004; Matthews & Meredith, 2004; Zhang, 2005). Upper level divergence associated with anomalous MJO heating interacts with the jet stream to form a Rossby wave source (Sardeshmukh & Hoskins, 1988) in the mid-latitudes. The propagation, and subsequent breaking, of these Rossby waves in the extratropics leads to changes in blocking (e.g., Henderson et al., 2016), jet dynamics (e.g., Bao & Hartmann, 2014; Kang & Tziperman, 2018) and weather regimes (e.g., Cassou, 2008; Lin et al., 2009, 2010; Mori & Watanabe, 2008; Riddle et al., 2013; Seo & Lee, 2017), which may be interpreted as teleconnection patterns.

Currently, deterministic weather prediction is skillful up to a lead time of approximately one to two weeks in the extratropics, however this lead time can be extended by considering the effects of modes such as the MJO (Kent et al., 2022; Nardi et al., 2020), Quasi-Biennial Oscillation (QBO; Nardi et al., 2020) and El Niño–Southern Oscillation (ENSO; Patricola et al., 2020). The signature teleconnection patterns produced by these modes provide predictive skill on sub-seasonal to seasonal time scales. This skill, however, is dependent on the ability of models to reproduce the mechanisms and variability of teleconnections over a range of time scales.

At present, even state-of-the-art General Circulation Models (GCMs) struggle to fully capture MJO teleconnections in their predictions (e.g., J. Wang et al., 2020a; J. Wang et al., 2020b). Though some are able to recreate the patterns of the teleconnections, these responses are almost universally too weak (Lin et al., 2021; Skinner et al., 2022; Vitart, 2017). This is a common feature across tropical–extratropical interactions in climate models and seasonal forecasts (Williams et al., 2023).

Supervision: Adrian J. Matthews, David P. Stevens

Validation: Daniel T. Skinner, David P. Stevens

Visualization: Daniel T. Skinner

Writing – original draft: Daniel T. Skinner

Writing – review & editing: Daniel T. Skinner, Adrian J. Matthews, David P. Stevens

ENSO is able to modulate the MJO (Chen et al., 2016; Hsu & Xiao, 2017; Kessler, 2001) and its teleconnections (Lee et al., 2019; Moon et al., 2011; Tseng et al., 2020) on seasonal to interannual time scales. However, there is little understanding of the variability of MJO teleconnections on decadal time scales. Furthermore, the extratropics have been shown to respond differently to remote forcing on interannual and decadal time scales (Seabrook et al., 2023).

In this study, evidence of decadal variability in the extratropical response to the MJO is presented, using ERA5 reanalysis data from 1974 (the start time of reliable MJO indices) to 2018. This variability is then compared with ENSO-modulated interannual variability. Finally, we discuss the impacts of changes in the response on the weather experienced in the extratropics.

2. Data and Methodology

The MJO varies on interannual (Chen et al., 2016; Hsu & Xiao, 2017; Kessler, 2001) and decadal (Fu et al., 2020; Jones & Carvalho, 2006; Wu et al., 2021) time scales. The extratropical response to the MJO is dependent on the background state of the atmosphere (Henderson et al., 2017), which can also vary on interannual and decadal time scales. These variations can be caused by changes in external forcing or in low-frequency modes of internal variability. Two key modes of variability are the Atlantic Multidecadal Variability (AMV; Kerr, 2000; Trenberth & Shea, 2006) and the Pacific Decadal Oscillation (PDO; Mantua et al., 1997; Mantua & Hare, 2002; Newman et al., 2016). Over the observational time period of 1974–2018, the AMV switches from its negative phase to positive phase around 1997. The PDO displays greater variability but moves from favoring its positive phase to negative phase, also switching around 1997 (Figure S1 in Supporting Information S1).

This leads us to consider changes in the extratropical response to the MJO between two non-overlapping segments: period one from 1974/75 to 1996/97, and period two from 1997/98 to 2017/18. Subsequent analysis is restricted to boreal winter (November–April) as this is when the MJO (and its teleconnections) are at their strongest (Jenney et al., 2019; Stan et al., 2017), and only considers full winter seasons. Due to an interruption in outgoing longwave radiation (OLR) data availability (Liebmann & Smith, 1996), there is no MJO index for 1978, so the 1977/78 and 1978/79 seasons are omitted. Hence our two time periods are of equal length at 21 winter seasons.

200-hPa streamfunction anomalies are derived from ERA5 wind data. Anomalies are calculated by removing the mean and first three harmonics of the annual cycle from the daily averaged ERA5 data. Annual cycles are calculated and removed separately for each time segment, so that the two periods may be considered independent samples. By removing separate annual cycles, the changes observed in the extratropical response to the MJO are due to changes in the interaction of the MJO with the mean state (i.e., the MJO teleconnection patterns), rather than changes in the mean state itself.

The MJO is diagnosed by the Realtime Multivariate MJO index, described by Wheeler and Hendon (2004), which is available from 1974 to present (Australian Bureau of Meteorology, 2021). The RMM index produces two values: a phase and amplitude. The phase, given by an integer between 1 and 8, signifies the zonal location of the centers of anomalous MJO convection. Phase 1 indicates enhanced convection over the western Indian Ocean, then, through eastward motion of the MJO, phases 2–3, 4–5, and 6–7 signify enhanced convection over the eastern Indian Ocean, Maritime Continent and western Pacific respectively. By Phase 8, the enhanced convection has moved into the eastern Pacific and dissipates, whilst simultaneously reforming in the western Indian Ocean. The amplitude indicates the relative strength of this anomalous convection.

Ten-day lagged composite maps of 200-hPa streamfunction anomaly are produced for each MJO phase, taking only days in which the MJO is "active" (defined as amplitude greater than 1). Note that all active days are included for each MJO event, not just the first day in each phase. Statistical significance in the difference between lagged composites in the two periods is assessed using a two-tailed, two-sample *t*-test at the 95% significance level.

To assess the impact of upper tropospheric circulation changes on meteorological conditions, 10-day lagged MJO composite maps of 850-hPa temperature and precipitation anomalies are also created. 850-hPa temperature anomalies are derived from daily-averaged ERA5 data. Precipitation anomalies are derived from CMAP pentad-mean data, which have been interpolated to daily data.

MJO teleconnection patterns are strongest in the winter (Northern) Hemisphere, so results are presented over this domain. Discussion will be made within the context of societal impacts, so will focus on regions which are densely populated, or which impact on key weather patterns such as the North Atlantic Oscillation (NAO).
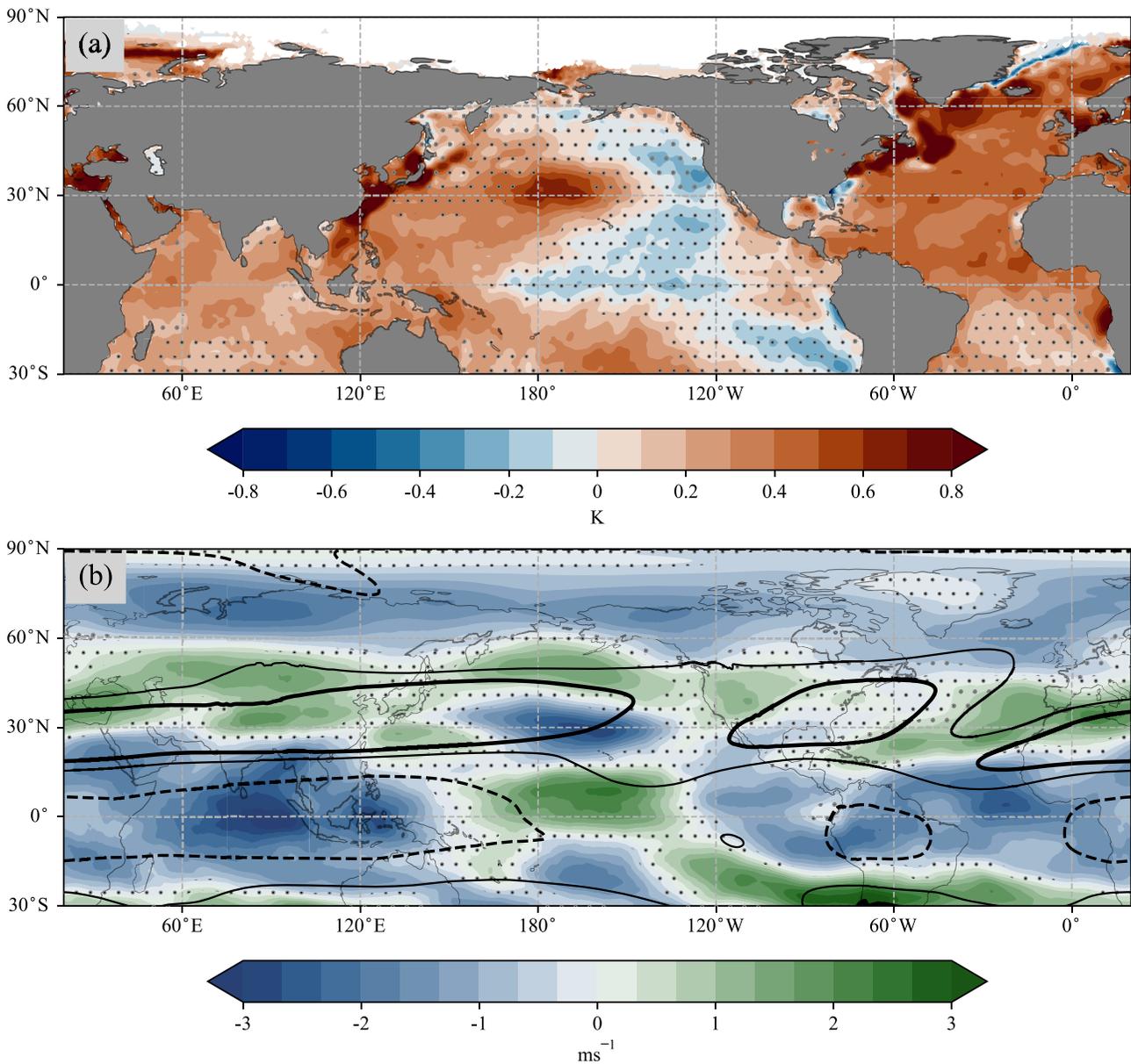
Figure 1. Change in boreal winter (November–April) mean (a) SST and (b) 200-hPa zonal wind: period two (1997/98–2017/18) minus period one (1974/75–1996/97). Stippling shows the regions in which this difference is not significant at the 95% confidence level, based on a two-sample, two-tailed *t*-test. Period two mean 200-hPa zonal wind is plotted at 0 m s^{-1} (dashed black contour), 20 m s^{-1} (thin black contour), and 30 m s^{-1} (thick black contour) in panel (b) for reference.

3. Decadal Variability of the Background State

Period one is characterized by the negative phase of the AMV and the positive phase of the PDO, whilst in period two the reverse is observed. The signatures of the AMV and PDO are visible in November–April mean HadISST sea surface temperatures (SSTs; Figure 1a). Whilst the change in AMV state is statistically significant at the 95% confidence level, the PDO SST pattern is only significant in the warm western and central North Pacific but not in the cold eastern North Pacific. There are changes in the upper tropospheric zonal wind (Figure 1b), where, as expected, there are changes in the subtropical jets (Matsumura & Horinouchi, 2016; Ruggieri et al., 2021). The northern hemisphere jet exhibits a general poleward shift in period two, particularly over the North Pacific.

Around the Maritime Continent there is evidence of a strengthened Gill-type response in the period two circulation due to SST warming in the Indian Ocean and western Pacific, which in turn leads to enhanced convection. This warming is consistent with the negative PDO (western Pacific; Mantua & Hare, 2002) and with a global

warming signal (Indian Ocean; Ruela et al., 2020). To the west of the Maritime Continent the equatorial easterly anomalies and off-equatorial westerly anomalies are consistent with twin anticyclones, indicating an enhanced equatorial Rossby wave response, whilst to the east of the Maritime Continent an enhanced equatorial Kelvin wave response can be seen in amplified westerlies near the equator.

Changes in SST patterns, both in the tropics and extratropics, and the corresponding changes in the upper troposphere together provide a different mean state with which the MJO and its teleconnections will interact. These changes are the combined result of both internal variability (i.e., the AMV and PDO) and long-term trends. In the present study, these changes are treated as a whole, due to the relatively short length of the data set. Future studies, making use of climate models, may have an opportunity to untangle the effects of individual mean state variations.

The stationary Rossby wavenumber, K_s, is defined as

$$K_s = \left(\frac{\beta - \overline{u}_{yy}}{\overline{u}} \right)^{\frac{1}{2}},$$

where $\overline{u}$ is the time-mean zonal wind, β is the meridional gradient of planetary vorticity, and $\overline{u}_{yy}$ is the meridional gradient of time-mean relative vorticity (with the meridional wind component neglected). Since Rossby waves usually propagate in the upper troposphere, the stationary Rossby wavenumber is calculated at 200 hPa. Rossby waves are refracted toward regions of high K_s (Dawson et al., 2011; Hoskins & Ambrizzi, 1993), so local maxima in K_s can be approximated as Rossby waveguides. This approximation relies on the crude assumption that the scale of the Rossby waves is much smaller than the scale of changes in the mean state (Hoskins & Ambrizzi, 1993; Hoskins & Karoly, 1981; Karoly, 1983), however it works well in a qualitative sense.

There is relatively little qualitative change in the North Atlantic waveguide (Figure 2), however a local minimum in K_s around 30°N, 140°W in period two diverts the North Pacific waveguide toward British Columbia and central Canada. During period one, however, this waveguide merges into the North Atlantic waveguide. The effect of this diversion in the waveguide is an amplified teleconnection over Canada and stronger Rossby wave response passing over Greenland into the North Atlantic.

4. Changes in the Upper Tropospheric Response to the MJO

4.1. Decadal Changes Between Periods One (1974/75–1996/97) and Two (1997/98–2017/18)

Upper tropospheric divergence associated with anomalous MJO convection forms an anticyclonic anomaly either side of the equator, spanning the convective center (Figure 3). The vorticity perturbation induced by this anticyclonic anomaly produces a stationary Rossby wave, characterized by alternating cyclonic and anticyclonic anomalies across the mid-latitudes. These broad features are visible in both period one and two; however, the strength and spatial structures of the Rossby wave trains have changed.

Over western North America there are substantial changes to the upper tropospheric circulation 10 days after MJO phases 1–2 and phases 5–6. In period two, the Rossby wave train initiated over the central North Pacific after MJO phases 1–2 extends over Canada, producing an cyclonic (anticyclonic) anomaly over British Columbia after phases 1–2 (5–6). This feature is not observed in period one. This change may be attributed to the deflection of Rossby waves into Canada as discussed in Section 3.

Continuing the Rossby wave train into the North Atlantic and Europe, we see the canonical NAO+ and NAO− responses (Cassou, 2008) after phases 3 and 6 respectively. Most notably, we see a strengthened anticyclonic anomaly (corresponding to a weakening of the Icelandic Low) in the North Atlantic after Phase 6. Whilst a broad cyclonic anomaly is present over southern Europe and the North Atlantic in period one, a strengthened and tilted cyclonic anomaly covers the entirety of Europe in period two. This anomalous low pressure center (Figure S5 in Supporting Information S1) will bring polar air masses across western Europe, which are colder than the air advected from eastern Europe in period one. It also represents a strengthening of the NAO− response that we would expect to see following Phase 6 (Cassou, 2008). Period two is characterized by AMV+ in the North Atlantic, which weakens the meridional temperature gradient across the North Atlantic, favoring NAO− conditions. This compounds and amplifies the NAO− response to MJO Phase 6.
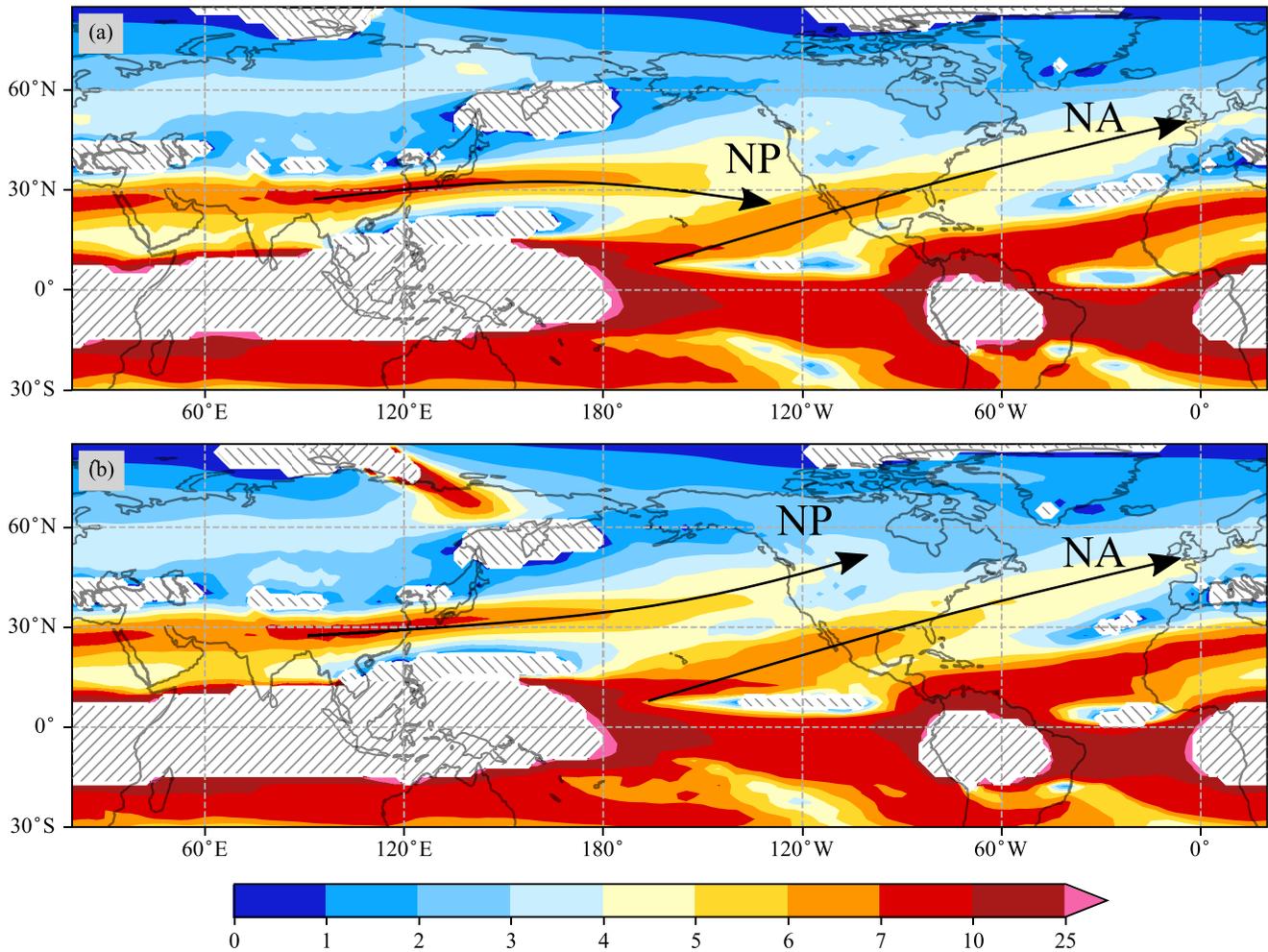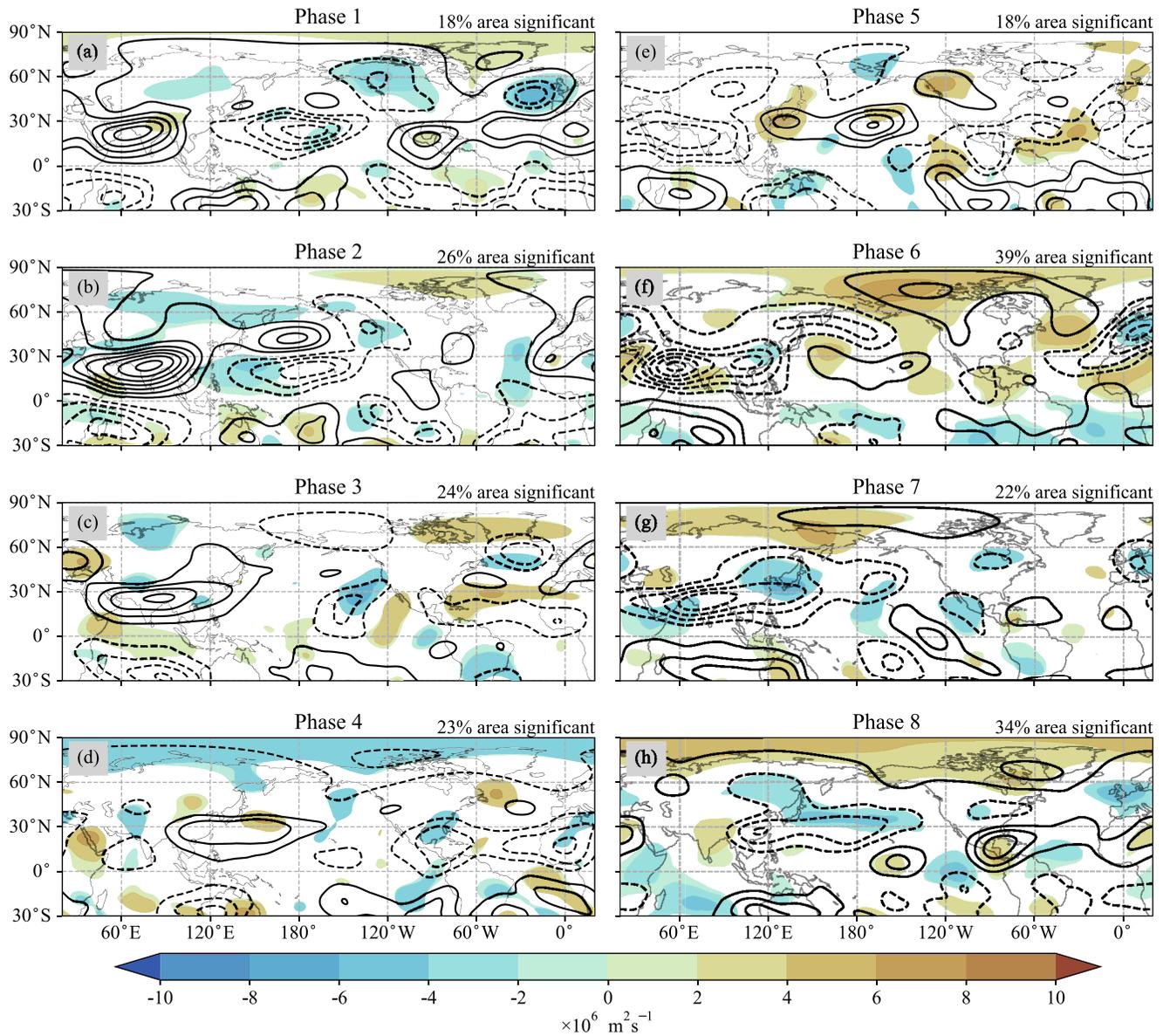
Figure 2. Boreal winter (November–April) 200-hPa stationary Rossby wavenumber, K_s, for (a) period one (1974/75–1996/97) and (b) period two (1997/98–2017/18). Regions in which K_s is undefined, and Rossby waves are evanescent—that is, when $\bar{u} < 0$ or $\beta - \bar{u}_{yy} < 0$—are denoted by hatching (////and \\\\ respectively). Rossby waves will tend to follow local maxima in K_s, hence these maxima can be qualitatively viewed as Rossby waveguides. Two key Rossby waveguides, the North Pacific (NP), and North Atlantic (NA), are labeled.

Overall, there are a considerable number of changes in the upper tropospheric circulation response to the MJO between periods 1 and 2. Now we compare these decadal variations against known interannual variability (Section 4.2) and assess the impacts of these changes (Section 5).

4.2. Interannual Changes Associated With ENSO

Whilst the MJO is the leading mode of tropical variability on sub-seasonal timescales, ENSO is the leading mode on interannual time scales. ENSO modulates MJO teleconnection patterns on interannual time scales (Lee et al., 2019; Moon et al., 2011; Roundy et al., 2010; Tseng et al., 2020), so it seems natural to compare this variability with the changes observed on decadal time scales. We expect to see some agreement because the ENSO SST pattern projects heavily onto the PDO SST pattern (the key difference being the relative strength of the North and tropical Pacific anomalies). On the other hand, there is evidence that the interaction between Pacific SST variability and the extratropics can be dependent on time scale (Seabrook et al., 2023). If the decadal variability discussed in Section 4.1 is an aliasing of the interannual ENSO variability, similar changes to the MJO response between El Niño and La Niña as between period one and two might be expected.

However, the spatial patterns of the decadal variability in the extratropical response to the MJO (Figure 3) and the interannual variability in the extratropical response to the MJO (Figures S2 and S3 in Supporting Information S1)

Figure 3. Lag 10-day composites of boreal winter (November–April) 200-hPa streamfunction anomaly for each of the eight MJO phases. Thick black contours represent period two, and shading shows the difference—period two (1997/98–2017/18) minus period one (1974/75–1996/97)—wherever this difference is significant at the 95% level. The contour interval for both the line and shaded contours is 2×10^6 m^2 s^{-1}, and dashed contours represent negative values. The zero contour has been omitted. The percentage of the spatial domain in which the difference is significant is stated in the top right of each panel.

take different forms. Even with the connection between the PDO and ENSO, there is no evidence that the observed decadal variability is due to aliasing of ENSO-modulated interannual variability.

5. Impacts of Changes to MJO Teleconnections

The observed changes in the upper tropospheric circulation response to the MJO between periods one and two will in turn lead to changes in the weather experienced in the extratropics. 10-day lagged composites of 850-hPa temperature anomaly are calculated using ERA5 data (Figures 4a–4d). Similarly, CMAP precipitation data are used to create 10-day lagged composites of precipitation anomaly (Figures 4e–4h). Due to the availability of CMAP data, precipitation composites were calculated from 1979/80 to 1996/97 for period one and from 1997/98 to 2015/16 for period two.

The response in lower tropospheric temperature to the MJO in period two (black contours in Figures 4a–4d) is generally qualitatively consistent with previous studies (e.g., Seo et al. (2016) Figure 1, Zhou et al. (2012) Figure
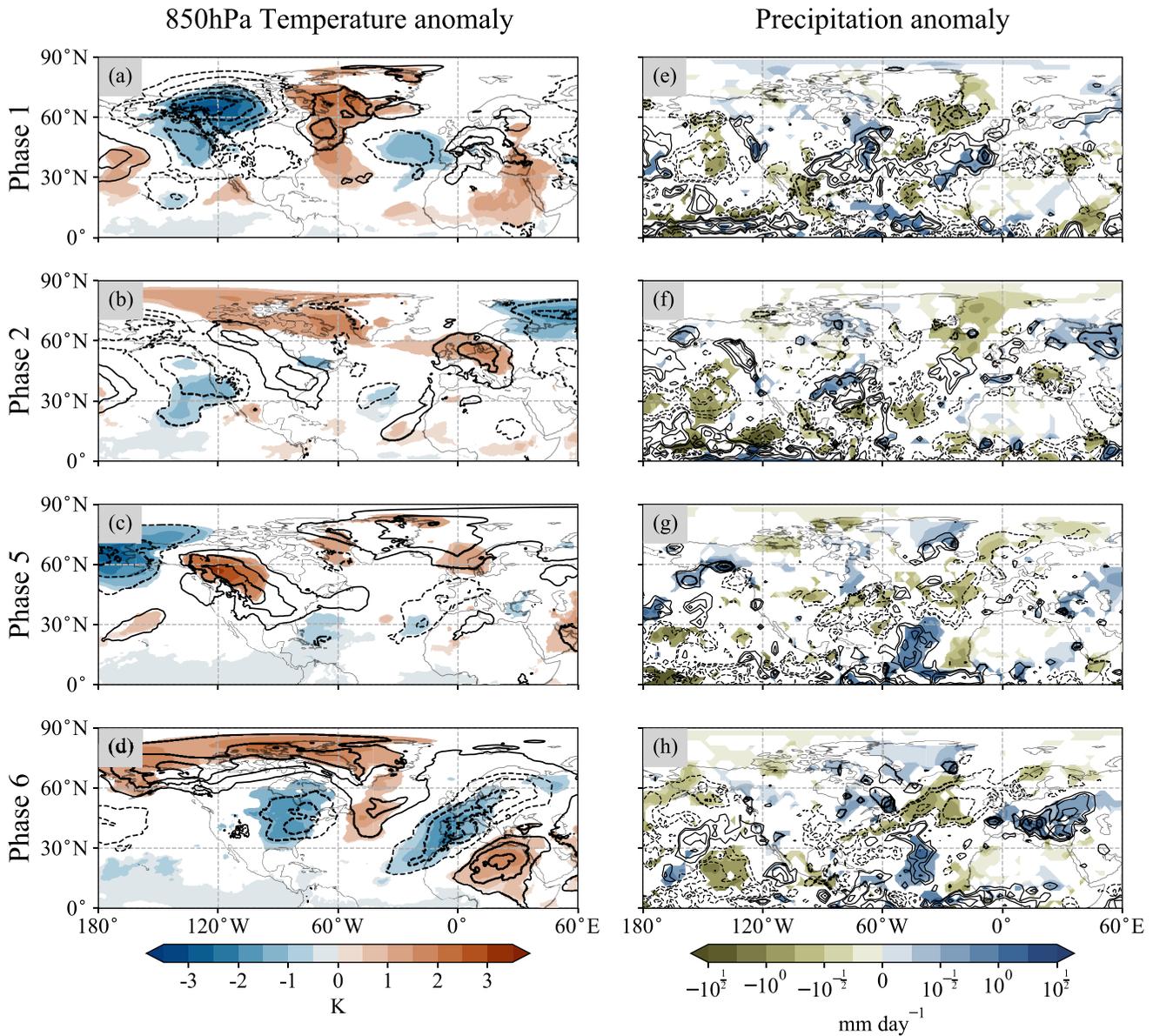
Figure 4. Change in 10-day lagged composites of (a–d) 850-hPa temperature and (e–h) precipitation anomalies over North America, Europe, and North Africa for MJO phases 1, 2, 5, and 6 (see Figure S4 in Supporting Information S1 for remaining phases). Difference—period two (1997/98–2017/18) minus period one (1974/75–1996/97)—is color shaded wherever it is significant at the 95% level, with change in precipitation anomaly plotted on a logarithmic scale. Period two composites are overlaid as black contours for reference. Solid contours represent positive values, dashed contours represent negative values and the zero contour has been omitted. Contour levels are the same for the line contours as they are for the shaded contours.

3, accounting for 1–2 phase shift as a result of the 10-day lag used here). There are some differences between the exact response to each MJO phase in these studies due to differences in the time domains and data sets used; however, our results match previous results to leading order.

There are significant and coherent changes in the lower tropospheric temperature response to the MJO from period one to period two. These changes are consistent with the differences observed in the upper tropospheric circulation response (and hence with the lower tropospheric circulation response, having confirmed equivalent barotropic behavior in the extratropics). Where responses have changed significantly between periods one and two, this usually corresponds to a strengthening of the teleconnection (since the shaded difference tends to be of the same sign as the black contours for period two).

Changes in the temperature response to the MJO over western Canada after MJO phases 1 and 5 are consistent with the changes in the upper tropospheric circulation and are exacerbated by the presence of the Rocky Mountains. In MJO Phase 1 there is a cold shift in the response. In period one there is anomalous south-easterly flow from the central United States to western Canada, whereas in period two colder air is advected westward from northern Canada. Conversely, after MJO Phase 5 warming is observed over western Canada in period two, as warmer air is transported north-westward from the midwestern United States.

Changes in the response to MJO Phase 6 will also have significant impacts on human populations across the northern hemisphere. Over eastern North America there is a shift to a cold anomaly, from anomalous southward advection from northern Canada rather than westward from the Atlantic. Interestingly, this cold anomaly is more often associated with the response to later MJO phases (e.g., Schreck et al., 2013), indicating a shift in the mechanisms of the response.

Across Europe, the strengthened and tilted cyclonic anomaly in period two has induced a strong cold anomaly. This feature is not present in period one but has a strength of -1.5 K in period two. The cold anomaly over Europe, paired with the eastern North American cold anomaly and warm anomaly over Greenland and Northern Canada bares considerable resemblance to the temperature pattern associated with the negative phase of the North Atlantic Oscillation (NAO$-$; C. Wang et al., 2010). Moreover, the average NAO index value at 10-day lag after MJO Phase 6 has increased in magnitude (i.e., has become more negative) by approximately 33% in period two, compared to period one. MJO Phase 6 is known to precede NAO$-$ (Cassou, 2008; Lin et al., 2009), so the strengthening of these patterns suggests a strengthened link between MJO Phase 6 and the NAO$-$ (Figure S5 in Supporting Information S1).

Precipitation anomalies (Figures 4e–4h) are less spatially coherent than the corresponding 850-hPa temperature anomalies. Nevertheless, statistically significant changes in the extratropical precipitation response to the MJO from period one to period two are observed in some locations. In particular, the cold shift over central and southern Europe in MJO Phase 6 is associated with a wet shift there, which is the opposite of what would usually be expected in boreal winter (Crhová & Holtanová, 2018; Madden & Williams, 1978). Over southern Europe this is due to the formation of a wet anomaly in period two, whereas in central/western Europe this is due to a switch from dry to slightly wet anomaly. An explanation for the change in southern Europe is that the cyclonic anomaly is associated with a low pressure anomaly. The center of this low pressure covers southern Europe in period two, whereas in period one the center is located off the west coast of North Africa. The low pressure over Europe will generally lead to cloudier, wetter weather and hence the positive precipitation anomaly.

6. Conclusions

Evidence has been found in ERA5 reanalysis data, showing that the extratropical response to the MJO changes on decadal time scales. ENSO is known to modulate MJO teleconnection patterns on interannual time scales, however the decadal variability we have observed differs from this ENSO-modulated variability and is not an example of aliasing over different time scales.

With only 4 decades of data, however, we are unable to conclusively attribute these changes to either external forcing or internal modes of variability. We hypothesize that low-frequency modes such as the AMV and PDO play a role in modulating MJO teleconnections, and by using climate models to increase our sample size we hope to examine this hypothesis further.

Changes in teleconnection patterns have impacts on meteorological conditions, particularly temperature and precipitation, which will directly affect human populations. These impacts are widespread, covering large portions of the extratropical Northern Hemisphere.

Skillful prediction of MJO teleconnections are vital to skillful seasonal forecasting in the extratropics (Kent et al., 2022), which in turn impacts on various industries (Palmer, 2002), including transportation (Karpechko et al., 2015; Palin et al., 2016), agriculture (Cantelaube & Terres, 2005; Challinor et al., 2005) and energy (Bloomfield et al., 2021; Clark et al., 2017). Finding clear evidence of decadal variability in the extratropical response to the MJO is a key step toward improved MJO-induced predictability in the extratropics and opens exciting opportunities for further refinement.

Data Availability Statement

All data used in the preparation of this manuscript are publicly available. ERA5 wind, geopotential and temperature data were provided by the Copernicus Climate Data Store (Copernicus Climate Change Service, 2023a, 2023b; Hersbach et al., 2020). HadISST SST data were provided by the Met Office Hadley Centre (Rayner et al., 2003; UK Met Office, 2022). The MJO index was accessed from the Australian Bureau of Meteorology (2021) and Nino 3.4 index from the US National Oceanic and Atmospheric Administration Earth System Research Laboratories (2022). The AMV index data were provided by the Climate Analysis Section, NCAR (Trenberth & Shea, 2006). The PDO index data were provided by the National Centers for Environmental Information, NOAA (Mantua, 1999, 2023). The NAO index data were provided by the National Oceanic and Atmospheric Administration Earth System Research Laboratories (2023). CMAP precipitation data (Xie & Arkin, 1997) were provided by the NOAA PSL.

References

Australian Bureau of Meteorology (2021). RMM data [Dataset]. Australian Government. Retrieved from http://www.bom.gov.au/climate/mjo

Bao, M., & Hartmann, D. L. (2014). The response to MJO-like forcing in a nonlinear shallow-water model. *Geophysical Research Letters*, *41*(4), 1322–1328. https://doi.org/10.1002/2013GL057683

Bloomfield, H. C., Brayshaw, D. J., Gonzalez, P. L. M., & Charlton-Perez, A. (2021). Sub-seasonal forecasts of demand and wind power and solar power generation for 28 European countries. *Earth System Science Data*, *13*(5), 2259–2274. https://doi.org/10.5194/essd-13-2259-2021

Cantelaube, P., & Terres, J.-M. (2005). Seasonal weather forecasts for crop yield modelling in Europe. *Tellus A: Dynamic Meteorology and Oceanography*, *57*(3), 476–487. https://doi.org/10.3402/tellusa.v57i3.14669

Cassou, C. (2008). Intraseasonal interaction between the Madden–Julian Oscillation and the North Atlantic Oscillation. *Nature*, *455*(7212), 523–527. https://doi.org/10.1038/nature07286

Challinor, A. J., Slingo, J. M., Wheeler, T. R., & Doblas–Reyes, F. J. (2005). Probabilistic simulations of crop yield over western India using the DEMETER seasonal hindcast ensembles. *Tellus A: Dynamic Meteorology and Oceanography*, *57*(3), 498–512. https://doi.org/10.3402/tellusa.v57i3.14670

Chen, X., Ling, J., & Li, C. (2016). Evolution of the Madden–Julian Oscillation in two types of El Niño. *Journal of Climate*, *29*(5), 1919–1934. https://doi.org/10.1175/JCLI-D-15-0486.1

Clark, R. T., Bett, P. E., Thornton, H. E., & Scaife, A. A. (2017). Skilful seasonal predictions for the European energy industry. *Environmental Research Letters*, *12*(2), 024002. https://doi.org/10.1088/1748-9326/aa57ab

Copernicus Climate Change Service. (2023a). ERA5 hourly data on pressure levels from 1940 to present [Dataset]. Copernicus Climate Change Service (C3S) Climate Data Store (CDS). https://doi.org/10.24381/cds.bd0915c6

Copernicus Climate Change Service. (2023b). ERA5 hourly data on single levels from 1940 to present [Dataset]. Copernicus Climate Change Service (C3S) Climate Data Store (CDS). https://doi.org/10.24381/cds.adbb2d47

Crhová, L., & Holtanová, E. (2018). Simulated relationship between air temperature and precipitation over Europe: Sensitivity to the choice of RCM and GCM. *International Journal of Climatology*, *38*(3), 1595–1604. https://doi.org/10.1002/joc.5256

Dawson, A., Matthews, A. J., & Stevens, D. P. (2011). Rossby wave dynamics of the North Pacific extra-tropical response to El Niño: Importance of the basic state in coupled GCMs. *Climate Dynamics*, *37*(1), 391–405. https://doi.org/10.1007/s00382-010-0854-7

Fu, Z., Hsu, P.-C., & Liu, F. (2020). Factors regulating the multidecadal changes in MJO amplitude over the twentieth century. *Journal of Climate*, *33*(22), 9513–9529. https://doi.org/10.1175/JCLI-D-20-0111.1

Henderson, S. A., Maloney, E. D., & Barnes, E. A. (2016). The influence of the Madden–Julian Oscillation on northern hemisphere winter blocking. *Journal of Climate*, *29*(12), 4597–4616. https://doi.org/10.1175/JCLI-D-15-0502.1

Henderson, S. A., Maloney, E. D., & Son, S.-W. (2017). Madden–Julian Oscillation Pacific teleconnections: The impact of the basic state and MJO representation in general circulation models. *Journal of Climate*, *30*(12), 4567–4587. https://doi.org/10.1175/JCLI-D-16-0789.1

Hersbach, H., Bell, B., Berrisford, P., Hirahara, S., Horányi, A., Muñoz Sabater, J., et al. (2020). The ERA5 global reanalysis. *Quarterly Journal of the Royal Meteorological Society*, *146*(730), 1999–2049. https://doi.org/10.1002/qj.3803

Hoskins, B. J., & Ambrizzi, T. (1993). Rossby wave propagation on a realistic longitudinally varying flow. *Journal of the Atmospheric Sciences*, *50*(12), 1661–1671. https://doi.org/10.1175/1520-0469(1993)050⟨1661:RWPOAR⟩2.0.CO;2

Hoskins, B. J., & Karoly, D. J. (1981). The steady linear response of a spherical atmosphere to thermal and orographic forcing. *Journal of the Atmospheric Sciences*, *38*(6), 1179–1196. https://doi.org/10.1175/1520-0469(1981)038⟨1179:TSLROA⟩2.0.CO;2

Hsu, P.-C., & Xiao, T. (2017). Differences in the initiation and development of the Madden–Julian Oscillation over the Indian Ocean associated with two types of El Niño. *Journal of Climate*, *30*(4), 1397–1415. https://doi.org/10.1175/JCLI-D-16-0336.1

Jenney, A. M., Nardi, K. M., Barnes, E. A., & Randall, D. A. (2019). The seasonality and regionality of MJO impacts on North American temperature. *Geophysical Research Letters*, *46*(15), 9193–9202. https://doi.org/10.1029/2019GL083950

Jiang, X., Adames, Á. F., Kim, D., Maloney, E. D., Lin, H., Kim, H., et al. (2020). Fifty years of research on the Madden–Julian Oscillation: Recent progress, challenges, and perspectives. *Journal of Geophysical Research: Atmospheres*, *125*(17), e2019JD030911. https://doi.org/10.1029/2019JD030911

Jones, C., & Carvalho, L. M. V. (2006). Changes in the activity of the Madden–Julian Oscillation during 1958–2004. *Journal of Climate*, *19*(24), 6353–6370. https://doi.org/10.1175/JCLI3972.1

Kang, W., & Tziperman, E. (2018). The MJO-SSW teleconnection: Interaction between MJO-forced waves and the midlatitude jet. *Geophysical Research Letters*, *45*(9), 4400–4409. https://doi.org/10.1029/2018GL077937

Karoly, D. J. (1983). Rossby wave propagation in a barotropic atmosphere. *Dynamics of Atmospheres and Oceans*, *7*(2), 111–125. https://doi.org/10.1016/0377-0265(83)90013-1

Karpechko, A. Y., Peterson, K. A., Scaife, A. A., Vainio, J., & Gregow, H. (2015). Skilful seasonal predictions of Baltic sea ice cover. *Environmental Research Letters*, *10*(4), 044007. https://doi.org/10.1088/1748-9326/10/4/044007

Kent, C., Scaife, A. A., & Dunstone, N. (2022). What potential for improving sub-seasonal predictions of the winter NAO? *Atmospheric Science Letters*, *24*(4), e1146. https://doi.org/10.1002/asl.1146

Kerr, R. A. (2000). A North Atlantic climate pacemaker for the centuries. *Science*, *288*(5473), 1984–1985. https://doi.org/10.1126/science.288.5473.1984

Kessler, W. S. (2001). EOF representations of the Madden–Julian Oscillation and its connection with ENSO. *Journal of Climate*, *14*(13), 3055–3061. https://doi.org/10.1175/1520-0442(2001)014⟨3055:EROTMJ⟩2.0.CO;2

Lee, R. W., Woolnough, S. J., Charlton-Perez, A. J., & Vitart, F. (2019). ENSO modulation of MJO teleconnections to the North Atlantic and Europe. *Geophysical Research Letters*, *46*(22), 13535–13545. https://doi.org/10.1029/2019GL084683

Liebmann, B., & Smith, C. (1996). Description of a complete (interpolated) outgoing longwave radiation dataset. *Bulletin of the American Meteorological Society*, *77*(6), 1275–1277.

Lin, H. (2022). The Madden–Julian Oscillation. *Atmosphere-Ocean*, *60*(3–4), 338–359. https://doi.org/10.1080/07055900.2022.2072267

Lin, H., Brunet, G., & Derome, J. (2009). An observed connection between the North Atlantic Oscillation and the Madden–Julian Oscillation. *Journal of Climate*, *22*(2), 364–380. https://doi.org/10.1175/2008JCLI2515.1

Lin, H., Brunet, G., & Fontecilla, J. S. (2010). Impact of the Madden–Julian Oscillation on the intraseasonal forecast skill of the North Atlantic Oscillation. *Geophysical Research Letters*, *37*(19), L19803. https://doi.org/10.1029/2010GL044315

Lin, H., Huang, Z., Hendon, H., & Brunet, G. (2021). NAO influence on the MJO and its prediction skill in the subseasonal-to-seasonal prediction models. *Journal of Climate*, *34*(23), 9425–9442. https://doi.org/10.1175/JCLI-D-21-0153.1

Madden, R. A., & Julian, P. R. (1971). Detection of a 40-50 day oscillation in the zonal wind in the tropical Pacific. *Journal of the Atmospheric Sciences*, *28*(5), 702–708. https://doi.org/10.1175/1520-0469(1971)028⟨0702:DOADOI⟩2.0.CO;2

Madden, R. A., & Julian, P. R. (1972). Description of global-scale circulation cells in the tropics with a 40-50 day period. *Journal of the Atmospheric Sciences*, *29*(6), 1109–1123. https://doi.org/10.1175/1520-0469(1972)029⟨1109:DOGSCC⟩2.0.CO;2

Madden, R. A., & Williams, J. (1978). The correlation between temperature and precipitation in the United States and Europe. *Monthly Weather Review*, *106*(1), 142–147. https://doi.org/10.1175/1520-0493(1978)106⟨0142:TCBTAP⟩2.0.CO;2

Mantua, N. J. (1999). The Pacific decadal Oscillation: A brief overview for non-specialists. *Encyclopedia of Environmental Change*.

Mantua, N. J., & Hare, S. R. (2002). The Pacific decadal Oscillation. *Journal of Oceanography*, *58*(1), 35–44. https://doi.org/10.1023/A:1015820616384

Mantua, N. J., Hare, S. R., Zhang, Y., Wallace, J. M., & Francis, R. C. (1997). A Pacific interdecadal climate oscillation with impacts on salmon production. *Bulletin of the American Meteorological Society*, *78*(6), 1069–1080. https://doi.org/10.1175/1520-0477(1997)078⟨1069:APICOW⟩2.0.CO;2

Matsumura, S., & Horinouchi, T. (2016). Pacific Ocean decadal forcing of long-term changes in the western Pacific subtropical high. *Scientific Reports*, *6*(1), 37765. https://doi.org/10.1038/srep37765

Matthews, A. J., Hoskins, B. J., & Masutani, M. (2004). The global response to tropical heating in the Madden—Julian Oscillation during the northern winter. *Quarterly Journal of the Royal Meteorological Society*, *130*(601), 1991–2011. https://doi.org/10.1256/qj.02.123

Matthews, A. J., & Meredith, M. P. (2004). Variability of Antarctic circumpolar transport and the Southern annular mode associated with the Madden–Julian Oscillation. *Geophysical Research Letters*, *31*(24), L24312. https://doi.org/10.1029/2004GL021666

Moon, J. Y., Wang, B., & Ha, K. J. (2011). ENSO regulation of MJO teleconnection. *Climate Dynamics*, *37*(5–6), 1133–1149. https://doi.org/10.1007/s00382-010-0902-3

Mori, M., & Watanabe, M. (2008). The growth and triggering mechanisms of the PNA: A MJO-PNA coherence. *Journal of the Meteorological Society of Japan*, *86*(1), 213–236. https://doi.org/10.2151/jmsj.86.213

Nardi, K. M., Baggett, C. F., Barnes, E. A., Maloney, E. D., Harnos, D. S., & Ciasto, L. M. (2020). Skillful all-season S2S prediction of U.S. precipitation using the MJO and QBO. *Weather and Forecasting*, *35*(5), 2179–2198. https://doi.org/10.1175/WAF-D-19-0232.1

National Oceanic, & Atmospheric Administration Earth System Research Laboratories. (2022). Niño 3.4 SST index [Dataset]. National Oceanic and Atmospheric Administration. Retrieved from https://psl.noaa.gov/gcos_wgsp/Timeseries/Data/nino34.long.data

National Oceanic and Atmospheric Administration Earth System Research Laboratories. (2023). North Atlantic Oscillation (NAO) [Dataset]. National Oceanic and Atmospheric Administration. Retrieved from https://psl.noaa.gov/data/timeseries/daily/NAO/

Newman, M., Alexander, M. A., Ault, T. R., Cobb, K. M., Deser, C., Lorenzo, E. D., et al. (2016). The Pacific decadal Oscillation, revisited. *Journal of Climate*, *29*(12), 4399–4427. https://doi.org/10.1175/JCLI-D-15-0508.1

Palin, E. J., Scaife, A. A., Wallace, E., Pope, E. C. D., Arribas, A., & Brookshaw, A. (2016). Skillful seasonal forecasts of winter disruption to the U.K. transport system. *Journal of Applied Meteorology and Climatology*, *55*(2), 325–344. https://doi.org/10.1175/JAMC-D-15-0102.1

Palmer, T. N. (2002). The economic value of ensemble forecasts as a tool for risk assessment: From days to decades. *Quarterly Journal of the Royal Meteorological Society*, *128*(581), 747–774. https://doi.org/10.1256/0035900021643593

Patricola, C. M., O'Brien, J. P., Risser, M. D., Rhoades, A. M., O'Brien, T. A., Ullrich, P. A., et al. (2020). Maximizing ENSO as a source of western US hydroclimate predictability. *Climate Dynamics*, *54*(1–2), 351–372. https://doi.org/10.1007/s00382-019-05004-8

Rayner, N. A., Parker, D. E., Horton, E. B., Folland, C. K., Alexander, L. V., Rowell, D. P., & Kaplan, A. (2003). Global analyses of sea surface temperature, sea ice, and night marine air temperature since the late nineteenth century. *Journal of Geophysical Research*, *108*(D14), 4407. https://doi.org/10.1029/2002JD002670

Riddle, E. E., Stoner, M. B., Johnson, N. C., L'Heureux, M. L., Collins, D. C., & Feldstein, S. B. (2013). The impact of the MJO on clusters of wintertime circulation anomalies over the North American region. *Climate Dynamics*, *40*(7–8), 1749–1766. https://doi.org/10.1007/s00382-012-1493-y

Roundy, P. E., MacRitchie, K., Asuma, J., & Melino, T. (2010). Modulation of the global atmospheric circulation by combined activity in the Madden–Julian Oscillation and the El Niño–Southern Oscillation during boreal winter. *Journal of Climate*, *23*(15), 4045–4059. https://doi.org/10.1175/2010JCLI3446.1

Ruela, R., Sousa, M., de Castro, M., & Dias, J. (2020). Global and regional evolution of sea surface temperature under climate change. *Global and Planetary Change*, *190*, 103190. https://doi.org/10.1016/j.gloplacha.2020.103190

Ruggieri, P., Bellucci, A., Nicolí, D., Athanasiadis, P. J., Gualdi, S., Cassou, C., et al. (2021). Atlantic multidecadal variability and North Atlantic jet: A multimodel view from the decadal climate prediction project. *Journal of Climate*, *34*(1), 347–360. https://doi.org/10.1175/JCLI-D-19-0981.1

Sardeshmukh, P. D., & Hoskins, B. J. (1988). The generation of global rotational flow by steady idealized tropical divergence. *Journal of the Atmospheric Sciences*, *45*(7), 1228–1251. https://doi.org/10.1175/1520-0469(1988)045⟨1228:TGOGRF⟩2.0.CO;2

Schreck, C. J., III, Cordeira, J. M., & Margolin, D. (2013). Which MJO events affect North American temperatures? *Monthly Weather Review*, *141*(11), 3840–3850. https://doi.org/10.1175/MWR-D-13-00118.1

Seabrook, M., Smith, D. M., Dunstone, N. J., Eade, R., Hermanson, L., Scaife, A. A., & Hardiman, S. C. (2023). Opposite impacts of interannual and decadal Pacific variability in the extratropics. *Geophysical Research Letters*, *50*(2), e2022GL101226. https://doi.org/10.1029/2022GL101226

Seo, K.-H., & Lee, H.-J. (2017). Mechanisms for a PNA-like teleconnection pattern in response to the MJO. *Journal of the Atmospheric Sciences*, *74*(6), 1767–1781. https://doi.org/10.1175/JAS-D-16-0343.1

Seo, K.-H., Lee, H.-J., & Frierson, D. M. W. (2016). Unraveling the teleconnection mechanisms that induce wintertime temperature anomalies over the northern hemisphere continents in response to the MJO. *Journal of the Atmospheric Sciences*, *73*(9), 3557–3571. https://doi.org/10.1175/JAS-D-16-0036.1

Skinner, D. T., Matthews, A. J., & Stevens, D. P. (2022). North Atlantic Oscillation response to the Madden—Julian Oscillation in a coupled climate model. *Weather*, *77*(6), 201–205. https://doi.org/10.1002/wea.4215

Stan, C., Straus, D. M., Frederiksen, J. S., Lin, H., Maloney, E. D., & Schumacher, C. (2017). Review of tropical–extratropical teleconnections on intraseasonal time scales. *Reviews of Geophysics*, *55*(4), 902–937. https://doi.org/10.1002/2016RG000538

Trenberth, K. E., & Shea, D. J. (2006). Atlantic hurricanes and natural variability in 2005. *Geophysical Research Letters*, *33*(12), L12704. https://doi.org/10.1029/2006GL026894

Tseng, K.-C., Maloney, E., & Barnes, E. A. (2020). The consistency of MJO teleconnection patterns on interannual time scales. *Journal of Climate*, *33*(9), 3471–3486. https://doi.org/10.1175/JCLI-D-19-0510.1

UK Met Office. (2022). Met Office Hadley centre observations datasets [Dataset]. Met Office. Retrieved from https://www.metoffice.gov.uk/hadobs/hadisst/data/download.html

Vitart, F. (2017). Madden–Julian Oscillation prediction and teleconnections in the S2S database. *Quarterly Journal of the Royal Meteorological Society*, *143*(706), 2210–2220. https://doi.org/10.1002/qj.3079

Wang, C., Liu, H., & Lee, S.-K. (2010). The record-breaking cold temperatures during the winter of 2009/2010 in the northern hemisphere. *Atmospheric Science Letters*, *11*(3), 161–168. https://doi.org/10.1002/asl.278

Wang, J., Kim, H., Kim, D., Henderson, S. A., Stan, C., & Maloney, E. D. (2020a). MJO teleconnections over the PNA region in climate models. Part I: Performance- and process-based skill metrics. *Journal of Climate*, *33*(3), 1051–1067. https://doi.org/10.1175/JCLI-D-19-0253.1

Wang, J., Kim, H., Kim, D., Henderson, S. A., Stan, C., & Maloney, E. D. (2020b). MJO teleconnections over the PNA region in climate models. Part II: Impacts of the MJO and basic state. *Journal of Climate*, *33*(12), 5081–5101. https://doi.org/10.1175/JCLI-D-19-0865.1

Wheeler, M. C., & Hendon, H. H. (2004). An all-season real-time multivariate MJO index: Development of an index for monitoring and prediction. *Monthly Weather Review*, *132*(8), 1917–1932. https://doi.org/10.1175/1520-0493(2004)132⟨1917:AARMMI⟩2.0.CO;2

Williams, N. C., Scaife, A. A., & Screen, J. A. (2023). Underpredicted ENSO teleconnections in seasonal forecasts. *Geophysical Research Letters*, *50*(5), e2022GL101689. https://doi.org/10.1029/2022GL101689

Wu, N., Li, Y., Li, J., Feng, L.-C., & Liu, F. (2021). Decadal changes of the intraseasonal oscillation during 1979—2016. *Advances in Climate Change Research*, *12*(6), 772–782. https://doi.org/10.1016/j.accre.2021.10.001

Xie, P., & Arkin, P. A. (1997). Global precipitation: A 17-year monthly analysis based on gauge observations, satellite estimates, and numerical model outputs. *Bulletin of the American Meteorological Society*, *78*(11), 2539–2558. https://doi.org/10.1175/1520-0477(1997)078⟨2539:GPAYMA⟩2.0.CO;2

Zhang, C. (2005). Madden–Julian Oscillation. *Reviews of Geophysics*, *43*(2), RG2003. https://doi.org/10.1029/2004RG000158

Zhou, S., L'Heureux, M., Weaver, S., & Kumar, A. (2012). A composite study of the MJO influence on the surface air temperature and precipitation over the continental United States. *Climate Dynamics*, *38*(7–8), 1459–1471. https://doi.org/10.1007/s00382-011-1001-9